Block-Type Antiferromagnetism in Single Chain Quasi-One-Dimensional $K_3Fe_2Se_4$

Fei Gao,[1,*] Nikhil Dhale,[1,*] Ling-Fang Lin,[2,†] Keith M. Taddei,[3,4] Yang Zhang,[5] Clarina Dela Cruz,[3] Elbio Dagotto,[2,5] and Bing Lv[1,6,‡]

[1]*Department of Physics, University of Texas at Dallas, Richardson, Texas 75080, USA*
[2]*Department of Physics and Astronomy, University of Tennessee, Knoxville, Tennessee 37996, USA*
[3]*Neutron Scattering Division, Oak Ridge National laboratory, Oak Ridge, Tennessee 37831, USA*
[4]*X-ray Science Division, Argonne National Laboratory, Lemont, Illinois 60439 USA*
[5]*Materials Science and Technology Division, Oak Ridge National Laboratory, Oak Ridge, Tennessee 37831, USA*
[6]*Department of Materials Science and Engineering, University of Texas at Dallas, Richardson, Texas 75080, USA*

(Received 14 October 2025; revised 28 February 2026; accepted 19 May 2026; published 24 June 2026)

One-dimensional (1D) structures provide a unique platform to study the correlated quantum interactions and phase transitions such as unconventional magnetism and superconducting states. Here, we report that iron chalcogenide $K_3Fe_2Se_4$ exhibits an unusual block-type canted antiferromagnetic (AFM) order with a clear single chain quasi-1D structure, which is structurally different from the two-leg ladder $BaFe_2Se_3$, through both experimental measurements and density matrix renormalization group (DMRG) calculations. The narrow bandgap semiconductor $K_3Fe_2Se_4$ has a quasi-1D edge-shared $FeSe_4$ tetrahedra chain structure and orders antiferromagnetically below 110 K. The magnetic moments couple antiferromagnetically along the quasi-1D chain direction of the b axis and form an up-down-down-up (↑-↓-↓-↑)–like spin structure with a commensurate propagation vector $\boldsymbol{k} = (0, 0, 0)$, where block-type spin ↑-↑ or ↓-↓ coupling are between the longer Fe-Fe bonds of the quasi-1D chain. DMRG results show that block antiferromagnetic state is stable in $K_3Fe_2Se_4$ and reveal that the block-ordered arrangement of $Fe^{2.5+}$ ions spins arise from the competition between ferromagnetic and AFM interaction in the presence of strong electronic correlation. Our research results not only report the discovery of a clear block-type canted antiferromagnetic structure in a real quasi-1D chain material but also provide a theoretical approach to understand the block-type antiferromagnetism in quasi-1D iron chalcogenides.

DOI: 10.1103/g8zx-gc2t

Introduction—One-dimensional (1D) material systems with correlated quantum interactions have attracted significant attention due to the intricate interplay among charge, orbital, spin and lattice degrees of freedom in low-dimensional phase space, resulting in rich physical phenomena. An extraordinary array of exotic states has been found in quasi-1D systems, such as charge density wave [1,2], Luttinger liquid [3,4], and quantum phase transition, etc. [5,6]. Quasi-1D spin chain systems provide ideal experimental platforms to test theoretical models such as classical Heisenberg ferromagnet and Ising-like antiferromagnet, as exemplified in $CsNiF_3$ [7], $SrM_2V_2O_8$ (M = Mn, Co) [8], $CsCoCl_3$ [9], and $BaCo_2V_2O_8$ [10], etc. The stripe-type or block-type antiferromagnetic (AFM) state is a plausible and often energetically favorable pattern in many correlated systems within approximate treatments. But so far strictly speaking it has not been realized in the real single chain quasi-1D materials, as it generally fails as an exact eigenstate of realistic Hamiltonians with full quantum many-body interactions due to fluctuations, competing energy scales and symmetrical constraints, etc. [11–13]. However, quasi-1D magnetic systems can exhibit stability through interchain coupling across the 1D and 2D dimensionality. One particularly interesting class of such systems is the ladder phase, which bridges the dimensional crossover from chains to square lattices by assembling chains side by side, as an alternative platform to study the competing electronic and magnetic orders [14,15]. The prime examples of such ladder phases are $SrCu_2O_3$, $Sr_{n-1}Cu_{n+1}O_{2n}$ family, and $BaFe_2X_3$ (X = S, Se) phases, which stay in between 1D and 2D [16–20]. Among these, the quasi-1D two-leg spin ladder $BaFe_2Se_3$ hosts an exotic Fe_4 block state, and such state could be changed to stripe-type AFM orders observed in the $BaFe_2S_3$ [20]. The block-type magnetic order highlights the strong low dimensional characteristics, localized electronic behavior, and complex magnetic interactions inherent to these systems. Understanding such block state is crucial for exploring magnetic transitions and potential superconductivity in iron-based materials. Therefore, it is particularly compelling to investigate block state in 1D

*These authors contributed equally to this work.
†Contact author: lflin@utk.edu
‡Contact author: blv@utdallas.edu

iron chalcogenides dominated by a single iron chain beyond the ladder phases.

In this Letter, we first report a true block-type AFM order in quasi-1D single-chain $K_3Fe_2Se_4$ through a combination of experimental measurements and density matrix renormalization roup (DMRG) calculations. $K_3Fe_2Se_4$ belongs to the ion mixed valence state iron chalcogenides $A_3Fe_2X_4$ (A = Na, K, Tl, X = S, Se) [21–25]. Interestingly, the magnetic order in these quasi-1D iron chalcogenides is rather intriguing. $Na_3Fe_2S_4$ and $Na_3Fe_2Se_4$ have a 1D AFM order within the chain, exhibiting a ferrimagnetic structure between the chains below 149 and 179 K, respectively [22], while $Tl_3Fe_2S_4$ has a collinear AFM structure below 90 K [21]. To date, only the structural determination has been reported for the compound $K_3Fe_2Se_4$ [25]. We found that this narrow bandgap semiconductor orders antiferromagnetically below 110 K. Moreover, neutron powder diffraction (NPD) experiments reveal the $Fe^{2.5+}$ ions spin exhibit an exotic up-down-down-up (↑-↓-↓-↑) arrangement along the single quasi-1D chain direction of the b axis, forming a block-type canted AFM structure results from the competing FM and AFM interactions in the presence of strong electronic correlations. Experimental and theoretical calculations details can be found in Supplemental Material [26].

Crystal structure and physical properties—$K_3Fe_2Se_4$ crystallizes in the centrosymmetric orthorhombic space group Pnma (No. 62) as with the two-leg ladder phase $BaFe_2Se_3$ but contains 1D zigzag chains of edge-linked distorted $FeSe_4$ tetrahedra [24,25], mimicking the fundamental building blocks for Fe-based superconductors [52–56]. The good Rietveld refinement results from powder x-ray diffraction (XRD) confirmed that the $K_3Fe_2Se_4$ crystallizes in the orthorhombic crystal structure of space group Pnma with $a = 7.427(7)$ Å, $b = 11.347(2)$ Å, and $c = 12.015(1)$ Å. The XRD pattern for the $K_3Fe_2Se_4$ and the corresponding structural refinement results are shown in Fig. S1 in Supplemental Material [26]. As shown in Fig. 1(a), the quasi-1D chains of Fe atoms are arranged along the b axis, with each Fe atom connected to the four nearest Se atoms to form a distorted $FeSe_4$ tetrahedra. Significantly, the bond lengths of adjacent Fe atoms on the quasi-1D Fe atom chain are not the same, which may lead to changes in the magnetic interaction between neighboring spins, resulting in competing magnetic interactions among them. Unlike the two-leg ladder chain in $BaFe_2Se_3$, $K_3Fe_2Se_4$ has a quasi-1D zigzag single chain of $FeSe_4$ tetrahedra [21–24]. In $K_3Fe_2Se_4$, the magnitude and coupling of spins in the Fe-Se tetrahedral are strongly influenced by Fe-Fe interactions within edge-sharing tetrahedra. The bond length of adjacent Fe-Fe in zigzag single chain $K_3Fe_2Se_4$ are different; the Fe atoms are connected in sequence with a short bond length of 2.833 Å and a long bond length of 3.037 Å, indicating the type of magnetic interaction between adjacent Fe spins may change as a result.

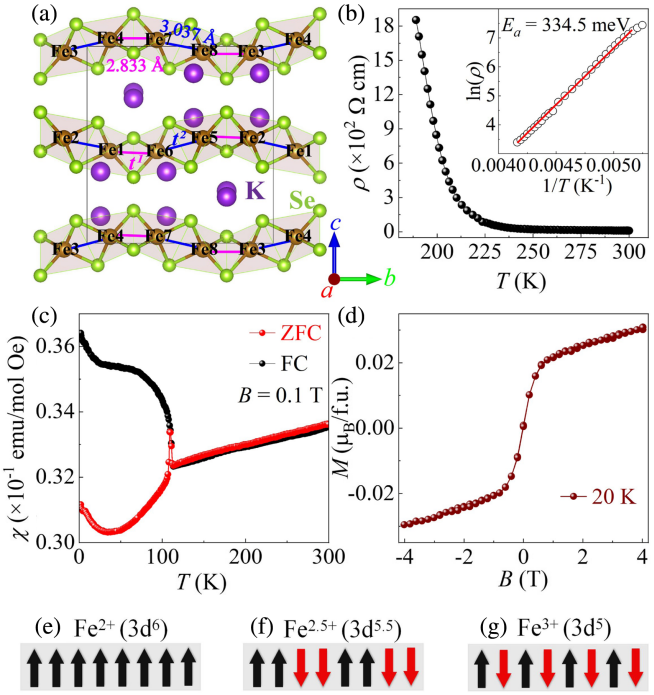

FIG. 1. (a) Crystal structure of quasi-1D single chain $K_3Fe_2Se_4$. The pink and blue lines represent longer and shorter Fe-Fe bonds in the zigzag iron chain, respectively. (b) Temperature-dependent electrical resistivity of $K_3Fe_2Se_4$. The inset shows the fitting result using the thermal activation model. (c) Temperature dependence of the ZFC and FC mode magnetic susceptibility with an applied field of 0.1 T. (d) Magnetic hysteresis loops at 20 K. Sketches of magnetic patterns with different electron occupations, corresponding to (e) Fe^{2+} ($3d^6$), (f) $Fe^{2.5+}$ ($3d^{5.5}$), and (g) Fe^{3+} ($3d^5$).

The temperature dependence of electrical resistivity from room temperature down to 190 K is shown in Fig. 1(b). Resistivity increases with decreasing temperature, indicating semiconducting behavior. The room-temperature value $\rho(300\ \mathrm{K})$ is about 10.4 Ω cm, which is comparable to other quasi-1D iron compounds with similar crystal structure, $BaFe_2Se_4$ and $BaFe_2Se_3$ [57,58]. The high temperature region of $\rho(T)$ was fit using the thermal activation model $\rho = \rho_0 \exp(E_a/k_BT)$, where k_B is the Boltzmann constant, ρ_0 is the prefactor, and E_a is the thermally activated energy [57,58]. The inset of Fig. 1(b) shows that the linear fitting of ln (ρ) vs $1/T$, resulting in $E_a = 334.5$ meV in the temperature range above 190 K, which is larger than in $BaFe_2Se_4$ and $BaFe_2Se_3$ [57,58], indicating $K_3Fe_2Se_4$ has stronger insulating properties.

The temperature-dependent magnetic susceptibility $\chi(T)$ from 2 to 300 K under zero-field cooled (ZFC) and field cooled (FC) procedures is shown in Fig. 1(c). In the high-temperature region, both the ZFC and FC $\chi(T)$ curves are identical. With decreasing temperature, the magnetic susceptibility shows a nearly liner decrease in amplitude with temperature, in stark contrast to the Curie-Weiss behavior

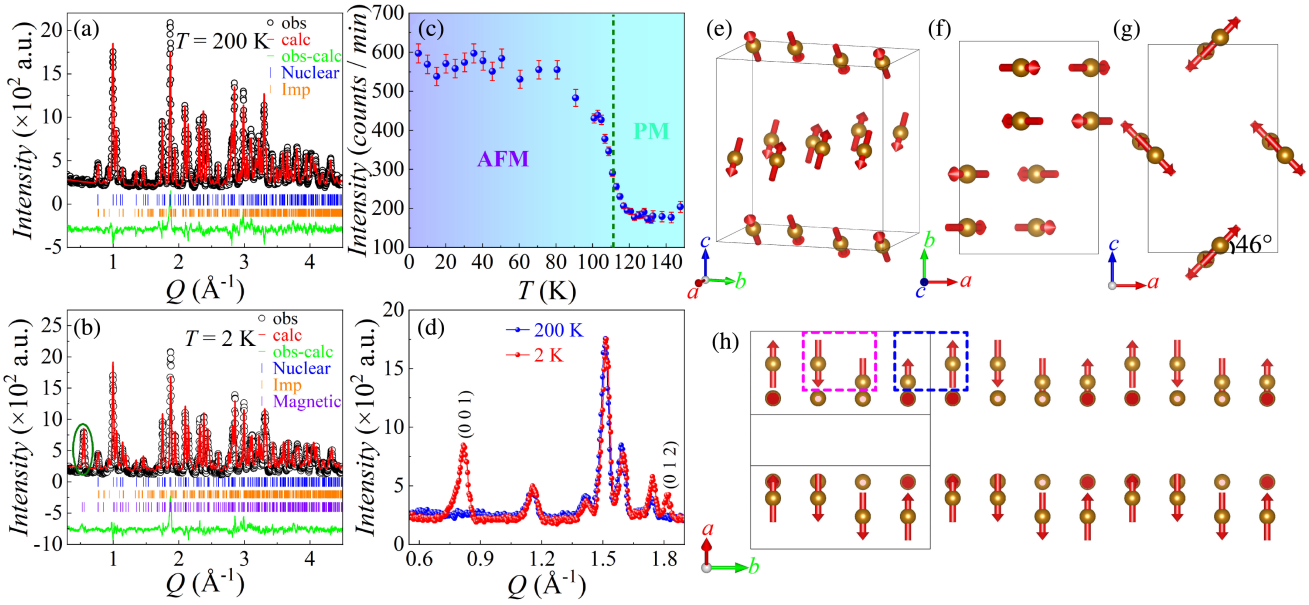

FIG. 2. Rietveld refinement of NPD data of $K_3Fe_2Se_4$ at (a) 200 K > T_N and (b) 2 K < T_N, respectively. The green circle indicates the first magnetic peak (0 0 1). (c) The intensity of the first magnetic peak (0 0 1) as a function of temperature. The green dotted line represents the antiferromagnetic transition temperature of 110 K. (d) Magnetic peaks evolved at $T = 2$ K as compared to no magnetic peaks at $T = 200$ K. (e) Zero-field magnetic structure of $K_3Fe_2Se_4$ at 2 K. (f) The spin structure of Fe couples in a unit cell of (0 0 1) plane. (g) Spin structure at magnetic Fe sites in a unit cell in-plane perpendicular to chain direction of b axis. (h) Block-type canted AFM spin alignment along the quasi-1D chain direction of b axis. The pink and blue dotted lines represent the parallel arrangement of $Fe^{2.5+}$ spins in each block-type structure. Black lines represent the crystal structure unit cell and red arrows represent the magnetic moment direction.

typically observed in localized spin systems. This unique feature is reminiscent of several two-leg ladder $SrCu_2O_3$ and $BaFe_2Se_3$, quasi-2D $La[O_{1-x}F_x]FeAs$ and $BaFe_2As_2$, and quasi-1D $RbFeSe_2$, $KFeS_2$, and Na_3FeSe_3 [16,18,59–63], which arises from distinct physical mechanisms despite their similar phenomenology. $SrCu_2O_3$ exhibits an exponential suppression of $\chi(T)$ due to a spin-gapped singlet ground state, while the Fe-based ladder, quasi-2D and quasi-1D Fe-chain systems display a gradual decrease of $\chi(T)$ driven by the growth of short-range AFM correlations or spin density wave fluctuations that transfer magnetic spectral weight away from the uniform channel. For an itinerant, multi-orbital quasi-1D $K_3Fe_2Se_4$, the enhancement of AFM correlations upon cooling primarily occurs at finite wave vectors, which suppresses the uniform magnetic susceptibility due to a redistribution of magnetic spectral weight, rather than enhancing it as in the localized-spin case. The quasi-one-dimensionality further strengthens short-range correlations without stabilizing long-range order, resulting in a gradual, nearly linear decrease of $\chi(T)$ over a broad temperature range. This experimental information also reminds us that $K_3Fe_2Se_4$ may become superconducting upon chemical doping or under pressure [18,64,65]. On further cooling, long-range AFM ordering appears below $T_N = 110$ K. The FC and ZFC curves have different behaviors below T_N, similar to $K_xFe_2Se_2$ and $BaFe_2Se_3$ [66,67], and the FC curves upturn in the low temperature is due to the magnetic moment increases with decreasing temperature, which will be discussed later. The isothermal magnetization curves $M(B)$ measured at 20 K, presented in Fig. 1(d), exhibits no hysteresis within the measuring magnetic field range. The magnetization rapidly increases with increasing magnetic field and tends to saturate under a low field of ±0.6 T. The value of magnetization at 4 T obtained from the isothermal magnetization curve is approximately $0.031\mu_B$/f.u., which is significantly reduced from $g_J J = 5\ \mu_B$ that is expected from a localized Fe^{3+} ion. This result is similar to $BaFe_2Se_4$ [57], indicating a strong itinerant character of the d electrons of the Fe atom in $K_3Fe_2Se_4$ [68], and this phenomenon also shows that the Fe ion in $K_3Fe_2Se_4$ does not occupy the trivalent state.

Magnetic mechanism—Here, we present the magnetic mechanism of the iron chain system of our focus. In the quasi-1D iron chalcogenide family, as shown in Figs. 1(e)–1(g), there are three typical magnetic patterns with different electron occupations, corresponding to Fe^{2+} ($3d^6$), $Fe^{2.5+}$ ($3d^{5.5}$), and Fe^{3+} ($3d^5$), respectively. As displayed in Fig. 1(e), Fe^{2+} ($3d^6$) is more conductive to stabilizing FM interaction along chain direction, such as $Ce_2O_2FeSe_2$ [69], which is caused by the recently proposed half-full mechanism [70]. Fe^{3+} ($3d^5$) is more conductive to promoting the formation of AFM coupling along the chain direction, such as $BaFe_2Se_4$ [57], which is induced by typical Anderson superexchange interaction [71]. As for the

intermediate case $K_3Fe_2Se_4$ in this Letter, both the half-full FM mechanism and Anderson AFM superexchange mechanism are potentially important [70–72], and their competition leads to the exotic block-type canted order with the ↑-↓-↓-↑ pattern, which will be explained later.

NPD and block-type magnetic order—To determine the magnetic structure of $K_3Fe_2Se_4$, temperature-dependent NPD experiments were carried out on HB-2A of the High Flux Isotope Reactor (HFIR) at the Oak Ridge National Laboratory (ORNL) using an incident wavelength of 2.41 Å [73,74]. NPD patterns collected at 200 and 2 K (i.e., above and below T_N) are illustrated in Figs. 2(a) and 2(b), respectively. The structural Rietveld refinement at 200 K confirms the orthorhombic structure of $K_3Fe_2Se_4$, resulting in lattice parameters $a = 7.414(7)$ Å, $b = 11.316(1)$ Å, and $c = 11.984(2)$ Å. This is consistent with room-temperature XRD results and indicates no extra structural transition with lowering temperature. During the Rietveld refinement of the NPD pattern, we found several structural peaks in the high-temperature NPD pattern unindexed by the main phase which can be indexed with a second minority phase with a different stoichiometry, $K_6Fe_4Se_8$, denoted as Imp, as shown in Fig. 2(a). Note that incorporating the Imp phase could improve the fitting quality, but it does not affect the determination of the magnetic structure. Where in the 2 K NPD pattern [Fig. 2(b)], we see the appearance of additional Bragg peaks due to long-range magnetic order. The position of the magnetic peaks can be seen in the partially enlarged neutron diffraction pattern in Fig. 2(d). As shown in Fig. 2(c), the temperature-dependent intensity of the first magnetic peak (0 0 1) presents a steep change at about 110 K, corresponding to the paramagnetic (PM) state to block AFM state transition. The Sarah and Bilbao Crystallographic Server were employed to determine the magnetic structure of $K_3Fe_2Se_4$ [75–78]. All the magnetic peaks could be indexed with the nuclear unit cell indicating a commensurate propagation vector $\boldsymbol{k} = (0, 0, 0)$. All allowed magnetic models were tested in Rietveld refinements, and magnetic space group Pn'ma' (BNS No. 62.448) was found to provide the best fit both visually and by statistical measurements, with the goodness-of-fit parameters $R_P = 16.0\%$, $R_{WP} = 18.4\%$, and $\chi^2 = 5.64\%$. Meanwhile, we also determined the magnetic structures at 110, 50, and 40 K through Rietveld refinement of the NPD data and found that the results are consistent with those observed at 2 K, as shown in Fig. S4 and Table S2 in Supplemental Material [26]. The magnetic structure of $K_3Fe_2Se_4$ is visualized in Figs. 2(e)–2(h), $K_3Fe_2Se_4$ has a block-type AFM structure, where the magnetic moments exhibit a ↑-↓-↓-↑ arrangement along the quasi-1D chain direction of the b axis. It is worth noting that the block-type spins ↑-↑ or ↓-↓ are located between the longer Fe-Fe bonds, as shown in Fig. 2(f). At 2 K, the value of the magnetic moment of each Fe atom is $3.33\mu_B$/Fe and lies in the ac plane, which is larger than that in the sister material $Tl_3Fe_2S_4$ [21]. In the ac plane, the adjacent spin of each layer is perpendicular to each other, and the tilting angle between each spin and the a/c axis is 46°, as shown in Fig. 2(g). As shown in Fig. 1(c) and Table S2 in Supplemental Material [26], the $\chi(T)$ in the FC mode shows an unusual increase below T_N, which agrees to the conclusion obtained by NPD experiments that the magnetic moment gradually increases with decreasing temperature in the magnetically ordered state. It should be noted that in this process, the tilting angle of the magnetic moment with the a/c axis gradually increases with decreasing temperature. As depicted in Fig. 2(h), the magnetic moments are arranged in an ↑-↓-↓-↑ sequence along the 1D zigzag iron chain of the b axis. The magnitude of the magnetic moment obtained by NPD is between the high spin states of a free Fe^{3+} and low spin states of a free Fe^{2+} [57,79], indicating a single state intermediate between Fe^{3+} and Fe^{2+} in $K_3Fe_2Se_4$. This block-type AFM order arrangement in the 1D zigzag single chain of $K_3Fe_2Se_4$ is quite different compared to typical block-type, stripe-type, or canted-type magnetic structures in quasi-1D linear chain iron chalcogenides [16,20,80–83]. In the two-leg spin ladder $BaFe_2Se_3$, the magnetic moments are in the ab plane, with every four spins arranged alternately as a block along the b axis [67,84]. Unlike the case of other alkali-metal analogs and $Tl_3Fe_2S_4$ [21] where magnetic orders usually show FM or AFM interactions, the AFM and FM interactions exist alternately along the 1D chain direction of $K_3Fe_2Se_4$, and a remarkable feature is that the FM spins arrangement are between longer curved Fe-Fe bonds of the folded iron chains. The longer Fe-Fe bond length creates conditions for the emergence of FM interactions. Unlike the $Tl_3Fe_2S_4$ whose magnetic moment is along the a axis [21], the magnetic moment of $K_3Fe_2Se_4$ is along the ac plane and has a tilting angle of 46° to the a/c axis, forming a block-type canted AFM structure. The different magnetic interactions may originate from changes in the $Fe^{2.5+}$ bonding configuration or the folded 1D chain here in the $K_3Fe_2Se_4$. Specifically, in $K_3Fe_2Se_4$, the dominance of selenium as a mediator in superexchange interactions may change to some extent.

DMRG calculation—As shown in Fig. 3(a), the conventional Anderson superexchange interaction arising from intraorbital hopping produces a strong AFM coupling in the half-filled system, leading to canonical staggered AFM state observed in the Fe^{3+} chain, such as $BaFe_2Se_4$ [57] and $RbFeSe_2$ [61] with d^5 configuration. However, the interorbital hopping could lead to a FM state [see Fig. 3(b)] between half-filled and full orbitals via Hund's coupling J_H, as recently discussed in the Fe^{2+} system $Ce_2O_2FeSe_2$ with d^6 configuration [70]. Here, our $K_3Fe_2Se_4$ case, with an average of 5.5 electrons of the iron d orbitals, has sizable intraorbital and interorbital hoppings, suggesting both AFM and FM tendencies could develop. From the Fe^{2+} to $Fe^{2.5+}$, the "effective" hole-doping effect in the

fully occupied orbitals reduces the FM tendency, leading to the strong competition between FM and AFM coupling, and to the possible block-type order with ↑-↓-↓-↑ pattern.

To better understand the block-type antiferromagnetic order [see Fig. 2(h)] in our NPD experiment of the $Fe^{2.5+}$ chain system $K_3Fe_2Se_4$, we also constructed a canonical three-orbital Hubbard model defined on a 1D chain lattice, by including the kinetic energy and interaction terms given by $H = H_k + H_{\rm int}$. The tight-binding kinetic component is

$$H_k = -\sum_{i\sigma\gamma\gamma'} t_{\gamma\gamma'}(c^\dagger_{i\sigma\gamma}c_{i+1\sigma\gamma'} + \text{H.c.}) + \sum_{i\gamma\sigma}\Delta_\gamma n_{i\gamma\sigma}, \quad (1)$$

where the first term $t_{\gamma\gamma'}$ represents the alternating nearest-neighbor (NN) hoppings $t^1_{\gamma\gamma'}$ and $t^2_{\gamma\gamma'}$ (see the detailed hopping matrix in Supplemental Material [26]) along the chain direction, starting from site $i = 0$, in the orbital space γ. Here, $t^1_{\gamma\gamma'}(t^2_{\gamma\gamma'})$ denotes the NN hoping from site i to $i+1$ on old (even) sites i. $c^\dagger_{i\sigma\gamma}(c_{i\sigma\gamma})$ is the standard creation (annihilation) operator, γ and γ' indicate the different orbitals, and σ is the z-axis spin projection. Δ_γ is the crystal-field splitting of different orbital γ.

The electronic interaction portion of the Hamiltonian includes the standard intraorbital Hubbard repulsion U, the electronic repulsion U' between electrons at different orbitals, the Hund's coupling J_H, and the on-site interorbital electron-pair hopping terms. Formally, it is written as

$$H_{\rm int} = U\sum_{i\gamma} n_{i\uparrow\gamma}n_{i\downarrow\gamma} + \left(U' - \frac{J_H}{2}\right)\sum_{\substack{i\\ \gamma<\gamma'}} n_{i\gamma}n_{i\gamma'} - 2J_H\sum_{\substack{i\\ \gamma<\gamma'}}\mathbf{S}_{i,\gamma}\cdot\mathbf{S}_{i,\gamma'} + J_H\sum_{\substack{i\\ \gamma<\gamma'}}(P^\dagger_{i\gamma}P_{i\gamma'} + \text{H.c.}), \quad (2)$$

where the standard relation $U' = U - 2J_H$ is assumed and the interorbital pair hopping $P_{i\gamma} = c_{i\downarrow\gamma}c_{i\uparrow\gamma}$. The relation $U' = U - 2J_H$ follows from the rotational invariance of the local Coulomb interaction in multiorbital systems and was originally derived within the Kanamori parametrization, which has been widely used in model calculations (see Ref. [85] for a discussion in the context of manganite as an example).

To confirm the above discussion, we measured the spin-spin correlation $S(r) = \langle \mathbf{S}_i \cdot \mathbf{S}_j \rangle$ and the spin structure factor $S(q)$ in our DMRG calculations, where the hoppings and crystal field splitting were obtained from $K_3Fe_2Se_4$ with two hopping matrices (more details can be found in Supplemental Material [26]). Here, we consider an electronic filling density $n = 3.5$ in our three-orbital DMRG calculations, rather than the nominal electronic configuration $d^{5.5}$ of $Fe^{2.5+}$. This choice follows the established theoretical treatments of iron chains, ladders, and layered superconductors with similar edge-sharing FeX_4 tetrahedron structure [70,86–91]. Such an approximation has been widely used in the theoretical studies of the real iron-based superconductor systems with Fe^{2+} or Fe^{3+} and is known to provide a good description of the physical properties [49,86,92,93].

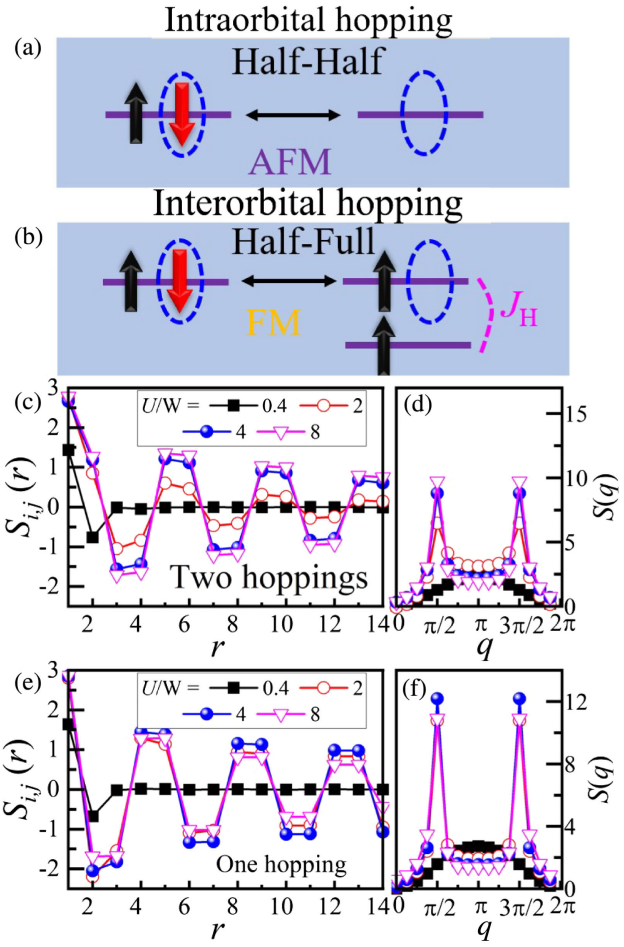

FIG. 3. Sketches of the superexchange picture between nearest neighbor sites for (a) half-half case with intraorbital hopping and (b) half-full case with interorbital hopping. Red arrows in the blue dashed circles indicate virtual hopping processes. Here, in the $K_3Fe_2Se_4$ case, both cases are potentially important, leading the block-type order with the ↑-↓-↓-↑ pattern. (c),(d) The DMRG results for $K_3Fe_2Se_4$ with chain lattice length $L = 16$: (c) spin-spin correlation $S(r) = \langle \mathbf{S}_i \cdot \mathbf{S}_j \rangle$ (with $r = |i - j|$ in real space) and (d) the spin structure factor $S(q)$, for different values of electronic correlations U/W, all at $J_H/U = 0.25$. (e),(f) The DMRG results for the uniform hopping [70] with chain lattice length $L = 16$: (e) spin-spin correlation $S(r)$ and (f) the spin structure factor $S(q)$, for different values of electronic correlations U/W, all at $J_H/U = 0.25$.

As displayed in Fig. 3(c), the spin-spin correlation $S(r)$ rapidly decays as the distance r increases at weak electronic correlation U/W region [see $U/W = 0.4$ as an example], where the distance is defined as $r = |i - j|$, with i and j site indexes. Correspondingly, the spin structure factor $S(q)$ does not show any obvious peaks in the reciprocal space,

indicating PM behavior in this region [see Figs. 3(c) and 3(d)]. By increasing U/W, the spin-spin correlation $S(r)$ shows clearly the formation of the block-type AFM with the antiferromagnetically coupled FM spin clusters (↑-↓-↓-↑ pattern), as displayed in Fig. 3(c). Moreover, the spin structure factor $S(q)$ also indicates a sharp peak at $q = \pi/2$, corresponding to the block-type AFM, as shown in Fig. 3(d). Our DMRG results suggest the block-type AFM state is robust in $K_3Fe_2Se_4$.

In addition, to better understand the possible origin of the block order in this $Fe^{2.5+}$ chain, we performed DMRG calculations for the chain model with a uniform NN hopping matrix [70] along the chain direction, using the same electronic filling $n = 3.5$ in the three-orbital model. The explicit form of the uniform hopping matrix can be found in Supplemental Material [26]. As displayed in Figs. 3(e) and 3(f), both spin-spin correlation $S(r)$ and spin structure factor $S(q)$ clearly indicate a block-type AFM magnetic coupling with ↑-↓-↓-↑ pattern along chain direction. This behavior is consistent with the results obtained in the three-orbital model within two bond alternation. Therefore, our results suggest that bond alternation is not the primary driving force for the formation of the block-type state in $K_3Fe_2Se_4$; rather, the block-type order of $Fe^{2.5+}$ originates from the competition between FM and AFM tendencies with electronic correlations. Thus, the bond alternation may result from the magnetostriction of the block-type order and is likely a secondary effect.

Notably, some quasi-1D ladder materials exhibit superconductivity under high pressure. For example, the two-leg ladder $Sr_{0.4}Ca_{13.6}Cu_{24}O_{41}$ shows a superconducting transition temperature ∼12 K under high pressure [94,95]. Similarly, pressure-induced superconductivity has been observed in the two-leg ladder compounds $BaFe_2S_3$ and $BaFe_2Se_3$ [18–20], spurring growing interest in quasi-1D iron chalcogenides. Beyond superconductivity, other intriguing phenomenon have been observed in ladder systems, such as spin density nodes [96], orbital ordering [96], ferroelectricity [97,98], orbitally selective Mott phases [99], and Peierls distortions, etc. [100,101]. In the future, it will be particularly interesting to explore the superconducting and related physical properties of quasi-1D single-chain $A_3Fe_2X_4$ and its element-substituted nonstoichiometric compounds.

Conclusion—Our Letter clearly demonstrates block-type AFM structure in the single chain quasi-1D $K_3Fe_2Se_4$. $K_3Fe_2Se_4$ is a narrow bandgap semiconductor and orders antiferromagnetically below 110 K. The $Fe^{2.5+}$ ions spin shows an ↑-↓-↓-↑ arrangement along the b axis in the direction of the quasi-1D chain to form a block-type canted AFM structure with a commensurate propagation vector $\boldsymbol{k} = (0, 0, 0)$, which is due to the competition between FM and AFM interactions in the presence of electronic correlations. This Letter provides a platform for future in-depth exploration of more exotic physical phenomena, e.g., whether superconductivity can emerge upon carrier doping, isovalent substitution, or under hydrostatic pressure in this family phases.

Acknowledgments—This work at the University of Texas at Dallas was supported by the U.S. Air Force Office of Scientific Research (No. FA9550-19-1-0037) National Science Foundation (No. DMR-DMREF-2324033 and No. ECCS-2516364), and Office of Naval Research (No. N00014-23-1-2020). The work of L.-F. L., Y. Z., and E. D. was supported by the U.S. Department of Energy, Office of Science, Basic Energy Sciences, Materials Sciences and Engineering Division. This research used resources at the High Flux Isotope Reactor, a DOE Office of Science User Facility operated by the Oak Ridge National Laboratory. Work was supported by the U.S. DOE Office of Science-Basic Energy Sciences under Contract No. DEAC02-06CH11357. The submitted manuscript has been created by UChicago Argonne, LLC, Operator of Argonne National Laboratory ("Argonne"). Argonne, a U.S. Department of Energy Office of Science laboratory, is operated under Contract No. DE-AC02-06CH11357. This manuscript has been also authored by UT-Battelle, LLC, under Contract No. DE-AC05-00OR22725 with the US Department of Energy (DOE).

Data availability—The data that supports the findings of this study are openly available [103].

[1] J. Hyun, Y. Lee, C.-y. Lim, G. Lee, J. Cha, Y. Ahn, M. Jho, S. Gim, M. Park, M. Hashimoto, D. Lu, Y. Kim, and S. Kim, Band-selective spin-charge separation across the charge density wave transition in quasi-1D $NbSe_3$, Phys. Rev. Lett. **134**, 206402 (2025).

[2] Y. Zhang, R. Zhou, H. Wu, J. S. Oh, S. Li, J. Huang, J. D. Denlinger, M. Hashimoto, D. Liu, S. K. Mo, K. F. Kelly, G. T. McCandless, J. Y. Chan, R. J. Birgeneau, B. Lv, G. Li, and M. Yi, Charge order induced Dirac pockets in the nonsymmorphic crystal $TaTe_4$, Phys. Rev. B **108**, 155121 (2023).

[3] N. Wakeham, A. F. Bangura, X. F. Xu, J.-F. Mercure, M. Greenblatt, and N. E. Hussey, Gross violation of the Wiedemann-Franz law in a quasi-one-dimensional conductor, Nat. Commun. **2**, 396 (2011).

[4] F. Wang, J. V. Alvarez, S.-K. Mo, J. W. Allen, G.-H. Gweon, J. He, R. Jin, D. Mandrus, and H. Höchst, New

luttinger-liquid physics from photoemission on $Li_{0.9}Mo_6O_{17}$, Phys. Rev. Lett. **96**, 196403 (2006).
[5] J. W. Huang, S. Li, C. Yoon, J. S. Oh, H. Wu, X. Liu, N. Dhale, Y.-F. Zhou, Y. Guo, Y. Zhang, M. Hashimoto, D. Liu, J. Denlinger, X. Wang, C. N. Lau, R. J. Birgeneau, F. Zhang, B. Lv, and M. Yi, Room-temperature topological phase transition in quasi-one-dimensional material Bi_4I_4, Phys. Rev. X **11**, 031042 (2021).
[6] S. Kimura, H. Yashiro, K. Okunishi, M. Hagiwara, Z. He, K. Kindo, T. Taniyama, and M. Itoh, Field-induced order-disorder transition in antiferromagnetic $BaCo_2V_2O_8$ driven by a softening of spinon excitation, Phys. Rev. Lett. **99**, 087602 (2007).
[7] J. Karadamoglou, N. Papanicolaou, X. Wang, and X. Zotos, Magnon dispersion and thermodynamics in $CsNiF_3$, Phys. Rev. B **63**, 224406 (2001).
[8] A. K. Bera, B. Lake, W.-D. Stein, and S. Zander, Magnetic correlations of the quasi-one-dimensional half-integer spin-chain antiferromagnets $SrM_2V_2O_8$ (M = Co, Mn), Phys. Rev. B **89**, 094402 (2014).
[9] T. Nakamura, Efficient monte carlo algorithm in quasi-one-dimensional Ising spin systems, Phys. Rev. Lett. **101**, 210602 (2008).
[10] B. Grenier, S. Petit, V. Simonet, E. Canévet, L.-P. Regnault, S. Raymond, B. Canals, C. Berthier, and P. Lejay, Longitudinal and transverse zeeman ladders in the Ising-like chain antiferromagnet $BaCo_2V_2O_8$, Phys. Rev. Lett. **114**, 017201 (2015).
[11] P. Corboz, T. M. Rice, and M. Troyer, Competing states in the t-J model: Uniform d-wave state versus stripe state, Phys. Rev. Lett. **113**, 046402 (2014).
[12] E. W. Huang, C. B. Mendl, S. X. Liu, S. Johnston, H.-C. Jiang, B. Moritz, and T. P. Devereaux, Numerical evidence of fluctuating in the normal state of high-T_C cuprate superconductors, Science **358**, 1161 (2017).
[13] Y. B. Zhang, C. Lane, J. W. Furness, B. Barbiellini, J. P. Perdew, R. S. Markiewicz, A. Bansil, and J. W. Sun, Competing stripe and magnetic phases in the cuprates from first principles, Proc. Natl. Acad. Sci. U.S.A. **117**, 68 (2020).
[14] E. Dagotto and T. M. Rice, Surprises on the way from one- to two-dimensional quantum magnets: The ladder materials, Science **271**, 618 (1996).
[15] E. Dagotto, Experiments on ladders reveal a complex interplay between a spin-gapped normal state and superconductivity, Rep. Prog. Phys. **62**, 1525 (1999).
[16] M. Azuma, Z. Hiroi, M. Takano, K. Ishida, and Y. Kitaoka, Observation of a spin gap in $SrCu_2O_3$ comprising spin-1/2 quasi-1D two-leg ladders, Phys. Rev. Lett. **73**, 3463 (1994).
[17] K. Ishida, Y. Kitaoka, K. Asayama, M. Azuma, Z. Hiroi, and M. Takano, Spin gap behavior in ladder-type of quasi-one-dimensional spin (S = 1/2) system $SrCu_2O_3$, J. Phys. Soc. Jpn. **63**, 3222 (1994).
[18] H. Takahashi, A. Sugimoto, Y. Nambu, T. Yamauchi, Y. Hirata, T. Kawakami, M. Avdeev, K. Matsubayashi, F. Du, C. Kawashima, H. Soeda, S. Nakano, Y. Uwatoko, Y. Ueda, T. J. Sato, and K. Ohgushi, Pressure-induced superconductivity in the iron-based ladder material $BaFe_2S_3$, Nat. Mater. **14**, 1008 (2015).
[19] T. Yamauchi, Y. Hirata, Y. Ueda, and K. Ohgushi, Pressure-induced mott transition followed by a 24 K superconducting phase in $BaFe_2S_3$, Phys. Rev. Lett. **115**, 24602 (2015).
[20] J. M. Caron, J. R. Neilson, D. C. Miller, A. Llobet, and T. M. McQueen, Iron displacements and magnetoelastic coupling in the antiferromagnetic spin-ladder compound $BaFe_2Se_3$, Phys. Rev. B **84**, 180409(R) (2011).
[21] D. Welz, P. Deppe, W. Schaefer, H. Sabrowsky, and M. Rosenberg, Magnetism of iron-sulfur tetrahedral frameworks in compounds with thallium chain structures, J. Phys. Chem. Solids **50**, 279 (1989).
[22] J. Ensling, P. Gütlich, and H. Spiering, Mössbauer and magnetic studies of mixed-valence linear chain compounds: $Na_3Fe_2S_4$ and $Na_3Fe_2Se_4$, Hyperfine Interact. **28**, 599 (1986).
[23] W. Bronger, U. Ruschewitz, and P. Müller, New ternary iron sulphides $A_3Fe_2S_4$ (A = K, Rb, Cs): Syntheses and crystal structures, J. Alloys Compd. **218**, 22 (1995).
[24] M. R. Harrison and M. G. Francesconi, Mixed-metal one-dimensional sulfides-A class of materials with differences and similarities to oxides, Coord. Chem. Rev. **225**, 451 (2011).
[25] W. Bronger, H. S. Genin, and P. Müller, K_3FeSe_3 and $K_3Fe_2Se_4$, two new compounds in the system K/Fe/Se, Z. Anorg. Allg. Chem. **625**, 247 (1999).
[26] See Supplemental Material at http://link.aps.org/supplemental/10.1103/g8zx-gc2t for sample synthesis, structure characterization, thermodynamics measurements, neutron diffraction experiments, density functional theory, and density matrix renormalization group calculations details, which includes Refs. [27–51].
[27] B. H. Toby and R. B. Von Dreele, GSAS-II: The genesis of a modern open-source all purpose crystallography software package, J. Appl. Crystallogr. **46**, 544 (2013).
[28] L. B. McCusker, R. B. Von Dreele, D. E. Cox, D. Louër, and P. Scardi, Rietveld refinement guidelines, J. Appl. Crystallogr. **32**, 36 (1999).
[29] J. Rodríguez-Carvajal, Recent advances in magnetic structure determination by neutron powder diffraction, Physica (Amsterdam) **192B**, 55 (1993).
[30] S. V. Gallego, E. S. Tasci, G. de la Flor, J. M. Perez-Mato, and M. I. Aroyo, Magnetic symmetry in the Bilbao Crystallographic Server: A computer program to provide systematic absences of magnetic neutron diffraction, J. Appl. Crystallogr. **45**, 1236 (2012).
[31] J. M. Perez-Mato, S. V. Gallego, E. S. Tasci, L. Elcoro, G. de la Flor, and M. I. Aroyo, Symmetry-based computational tools for magnetic crystallography, Annu. Rev. Mater. Res. **45**, 217 (2015).
[32] A. S. Wills, A new protocol for the determination of magnetic structures using simulated annealing and representational analysis (SARAh), Physica (Amsterdam) **276B**, 680 (2000).
[33] A. A. Mostofi, J. R. Yates, Y. S. Lee, I. Souza, D. Vanderbilt, and N. Marzari, Wannier90: A tool for obtaining maximally-localized Wannier functions, Comput. Phys. Commun. **178**, 685 (2007).
[34] G. Kresse and J. Hafner, Ab initio molecular dynamics for liquid metals, Phys. Rev. B **47**, 558(R) (1993).

[35] G. Kresse and J. Furthmüller, Efficient iterative schemes for ab initio total-energy calculations using a plane-wave basis set, Phys. Rev. B **54**, 11169 (1996).
[36] P. E. Blöchl, Projector augmented-wave method, Phys. Rev. B **50**, 17953 (1994).
[37] J. P. Perdew, K. Burke, and M. Ernzerhof, Generalized gradient approximation made simple, Phys. Rev. Lett. **77**, 3865 (1996).
[38] L. F. Lin, Y. Zhang, G. Alvarez, A. Moreo, and E. Dagotto, Origin of insulating ferromagnetism in iron oxychalcogenide $Ce_2O_2FeSe_2$, Phys. Rev. Lett. **127**, 077204 (2021).
[39] S. R. White, Density matrix formulation for quantum renormalization groups, Phys. Rev. Lett. **69**, 2863 (1992).
[40] S. R. White, Density-matrix algorithms for quantum renormalization groups, Phys. Rev. B **48**, 10345 (1993).
[41] G. Alvarez, The density matrix renormalization group for strongly correlated electron systems: A generic implementation, Comput. Phys. Commun. **180**, 1572 (2009).
[42] https://g1257.github.io/dmrgPlusPlus/.
[43] Q. Luo, G. Martins, D.-X. Yao, M. Daghofer, R. Yu, A. Moreo, and E. Dagotto, Neutron and ARPES constraints on the couplings of the multiorbital Hubbard model for the iron pnictides, Phys. Rev. B **82**, 104508 (2010).
[44] M. Daghofer, A. Nicholson, A. Moreo, and E. Dagotto, Three orbital model for the iron-based superconductors, Phys. Rev. B **81**, 014511 (2010).
[45] Y. Zhang, L.-F. Lin, G. Alvarez, A. Moreo, and E. Dagotto, Magnetic states of the quasi-one-dimensional iron chalcogenide Ba_2FeSe_3, Phys. Rev. B **104**, 125122 (2021).
[46] J. Herbrych, N. Kaushal, A. Nocera, G. Alvarez, A. Moreo, and E. Dagotto, Spin dynamics of the block orbital-selective Mott phase, Nat. Commun. **9**, 3736 (2018).
[47] J. Rincón, A. Moreo, G. Alvarez, and E. Dagotto, Exotic magnetic order in the orbital-selective Mott regime of multiorbital systems, Phys. Rev. Lett. **112**, 106405 (2014).
[48] S. Li, N. Kaushal, Y. Wang, Y. Tang, G. Alvarez, A. Nocera, T. A. Maier, E. Dagotto, and S. Johnston, Nonlocal correlations in the orbital selective Mott phase of a one-dimensional multiorbital Hubbard model, Phys. Rev. B **81**, 014511 (2010).
[49] L. F. Lin, Y. Zhang, G. Alvarez, M. A. McGuire, A. F. May, A. Moreo, and E. Dagotto, Stability of the interorbital-hopping mechanism for ferromagnetism in multi-orbital Hubbard models, Commun. Phys. **6**, 199 (2023).
[50] E. E. McCabe, C. Stock, J. L. Bettis, Jr., M.-H. Whangbo, and J. S. O. Evans, Magnetism of the Fe^{2+} and Ce^{3+} sublattices in $Ce_2O_2FeSe_2$: A combined neutron powder diffraction, inelastic neutron scattering, and density functional study, Phys. Rev. B **90**, 235115 (2014).
[51] L. F. Lin, Y. Zhang, G. Alvarez, J. Herbrych, A. Moreo, and E. Dagotto, Prediction of orbital-selective Mott phases and block magnetic states in the quasi-one-dimensional iron chain $Ce_2O_2FeSe_2$ under hole and electron doping, Phys. Rev. B **105**, 075119 (2022).
[52] K. Sasmal, B. Lv, B. Lorenz, A. M. Guloy, F. Chen, Y.-Y. Xue, and C.-W. Chu, Superconducting Fe-based compounds $(A_{1-x}Sr_x)Fe_2As_2$ with A = K and Cs with transition temperatures up to 37 K, Phys. Rev. Lett. **101**, 107007 (2008).
[53] J. H. Tapp, Z. J. Tang, B. Lv, K. Sasmal, B. Lorenz, Paul C. W. Chu, and A. M. Guloy, LiFeAs: An intrinsic FeAs-based superconductor with $T_C = 18$ K, Phys. Rev. B **78**, 060505(R) (2008).
[54] L. Z. Deng, B. Lv, K. Zhao, F. Y. Wei, Y. Y. Xue, Z. Wu, and C. W. Chu, Evidence for defect-induced superconductivity up to 49 K in $(Ca_{1-x}R_x)Fe_2As_2$, Phys. Rev. B **93**, 054513 (2016).
[55] B. Lv, L. Z. Deng, M. Gooch, F. Y. Wei, Y. Y. Sun, J. K. Meen, Y.-Y. Xue, B. Lorenz, and C.-W. Chu, Unusual superconducting state at 49 K in electron-doped $CaFe_2As_2$ at ambient pressure, Proc. Natl. Acad. Sci. U.S.A. **108**, 15705 (2011).
[56] K. Sasmal, B. Lv, Z. J. Tang, F. Chen, Y. Y. Xue, B. Lorenz, A. M. Guloy, and C. W. Chu, Unusual doping dependence of superconductivity in Na_yFeAs, Phys. Rev. B **79**, 184516 (2009).
[57] X. Y. Liu, K. M. Taddei, S. Li, W. H. Liu, N. Dhale, R. Kadado, D. Berman, C. D. Cruz, and B. Lv, Canted antiferromagnetism in the quasi-one-dimensional iron chalcogenide $BaFe_2Se_4$, Phys. Rev. B **102**, 180403(R) (2020).
[58] H. C. Lei, H. Ryu, A. I. Frenkel, and C. Petrovic, Anisotropy in $BaFe_2Se_3$ single crystals with double chains of FeSe tetrahedra, Phys. Rev. B **84**, 214511 (2011).
[59] Y. Kamihara, T. Watanabe, M. Hirano, and H. Hosono, Iron-based layered superconductor $La[O_{1-x}F_x]FeAs$ (x = 0.05-0.12) with $T_C = 26$ K, J. Am. Chem. Soc. **130**, 3296 (2008).
[60] M. Rotter, M. Tegel, and D. Johrendt, I. Schellenberg, W. Hermes, R. Pottgen, Spin-density-wave anomaly at 140 K in the ternary iron arsenide $BaFe_2As_2$, Phys. Rev. B **78**, 020503(R) (2008).
[61] Z. Seidov, H.-A. Krug von Nidda, V. Tsurkan, I. G. Filippova, A. Günther, T. P. Gavrilova, F. G. Vagizov, A. G. Kiiamov, L. R. Tagirov, and A. Loidl, Spin-density-wave anomaly at 140 K in the ternary iron arsenide $BaFe_2As_2$, Phys. Rev. B **94**, 134414 (2016).
[62] S. K. Tiwary and S. Vasudevan, Regular versus alternating $(FeSe_4)n$ chains: Magnetism in $KFeS_2$ and $CsFeS_2$, Phys. Rev. B **56**, 7812 (1997).
[63] W. Bronger and P. Müller, The magnetochemical characterization of the bonding features in ternary chalcogenides of manganese, iron and cobalt with low dimensional structural units, J. Alloys Compd. **246**, 27 (1997).
[64] M. Rotter, M. Tegel, and D. Johrendt, Superconductivity at 38 K in the iron arsenide $(Ba_{1-x}K_x)Fe_2As_2$, Phys. Rev. Lett. **101**, 107006 (2008).
[65] S. A. J. Kimber, A. Kreyssig, Y.-Z. Zhang, H. O. Jeschke, R. Valenti, F. Yokaichiya, E. Colombier, J. Q. Yan, T. C. Hansen, T. Chatterji, R. J. McQueeney, P. C. Canfield, A. I. Goldman, and D. N. Argyriou, Similarities between structural distortions under pressure and chemical doping in superconducting $BaFe_2As_2$, Nat. Mater. **8**, 471 (2009).
[66] H. Ryu, H. C. Lei, A. I. Frenkel, and C. Petrovic, Local structural disorder and superconductivity in $K_xFe_{2-y}Se_2$, Phys. Rev. B **85**, 224515 (2012).
[67] Y. Nambu, K. Ohgushi, S. Suzuki, F. Du, M. Avdeev, Y. Uwatoko, K. Munakata, H. Fukazawa, S. X. Chi, Y. Ueda, and T. S. Sato, Block magnetism coupled with local

distortion in the iron-based spin-ladder compound $BaFe_2Se_3$, Phys. Rev. B **85**, 064413 (2012).
[68] K. Motizuki, T. Korenari, and M. Shirai, Electronic band structures and magnetism of intermetallic Cu_2 Sb-type manganese compounds MnAlGe and MnGaGe, J. Magn. Magn. Mater. **104**, 1923 (1992).
[69] E. E. McCabe, C. Stock, J. L. Bettis, Jr., M.-H. Whangbo, and J. S. O. Evans, Magnetism of the Fe^{2+} and Ce^{3+} sublattices in $Ce_2O_2FeSe_2$: A combined neutron powder diffraction, inelastic neutron scattering, and density functional study, Phys. Rev. B **90**, 235115 (2014).
[70] L. F. Lin, Y. Zhang, G. Alvarez, A. Moreo, and E. Dagotto, Origin of insulating ferromagnetism in iron oxychalcogenide $Ce_2O_2FeSe_2$, Phys. Rev. Lett. **127**, 077204 (2021).
[71] Y. Zhang, P. Laurell, G. Alvarez, A. Moreo, T. A. Maier, L.-F. Lin, and E. Dagotto, Intertwined charge, spin, and orbital degrees of freedom under electronic correlations in the one-dimensional Fe^{3+} chalcogenide chain, arXiv: 2507.09870.
[72] L. F. Lin, Y. Zhang, G. Alvarez, J. Herbrych, A. Moreo, and E. Dagotto, Prediction of orbital-selective Mott phases and block magnetic states in the quasi-one-dimensional iron chain $Ce_2O_2FeSe_2$ under hole and electron doping, Phys. Rev. B **105**, 075119 (2022).
[73] V. O. Garlea, B. C. Chakoumakos, S. A. Moore, G. B. Taylor, T. Chae, R. G. Maples, R. A. Riedel, G. W. Lynn, and D. L. Selby, A suite-level review of the neutron powder diffraction instruments at Oak Ridge National Laboratory, Appl. Phys. A **99**, 531 (2010).
[74] S. Calder, K. An, R. Boehler, C. R. Dela Cruz, M. D. Frontzek, M. Guthrie, B. Haberl, A. Huq, S. A. J. Kimber, J. Liu, J. J. Molaison, J. Neuefeind, K. Page, A. M. dos Santos, K. M. Taddei, C. Tulk, and M. G. Tucker, Recent advances in magnetic structure determination by neutron powder diffraction, Rev. Sci. Instrum. **89**, 092701 (2018).
[75] J. Rodríguez-Carvajal, Smmetry-based computational tools for magnetic crystallography, Physica (Amsterdam) **192B**, 55 (1993).
[76] S. V. Gallego, E. S. Tasci, G. de la Flor, J. M. Perez-Mato, and M. I. Aroyo, Representation analysis of magnetic structures, J. Appl. Crystallogr. **45**, 1236 (2012).
[77] E. F. Bertaut, Representation analysis of magnetic structures, Acta Crystallogr. Sect. A **24**, 217 (1968).
[78] A. S. Wills, A new protocol for the determination of magnetic structures using simulated annealing and representational analysis (SARAh), Physica (Amsterdam) **276B**, 680 (2000).
[79] L. S. Li, L. L. Zheng, B. A. Frandsen, A. D. Christianson, D.-X. Yao, M. Wang, and R. J. Birgeneau, Spin dynamics of the spin-chain antiferromagnets $RbFeS_2$, Phys. Rev. B **104**, 224419 (2021).
[80] T. Yamauchi, Y. Hirata, Y. Ueda, and K. Ohgushi, Pressure-induced Mott transition followed by a 24 K superconducting phase in $BaFe_2S_3$, Phys. Rev. Lett. **115**, 246402 (2015).
[81] J. Ying, H. C. Lei, C. Petrovic, Y. Xiao, and V. V. Struzhkin, Interplay of magnetism and superconductivity in the compressed Fe-ladder compound $BaFe_2Se_3$, Phys. Rev. B **95**, 241109(R) (2017).
[82] J. M. Caron, J. R. Neilson, D. C. Miller, K. Arpino, A. Llobet, and T. M. McQueen, Orbital-selective magnetism in the spin-ladder iron selenides $Ba_{1-x}K_xFe_2Se_3$, Phys. Rev. B **85**, 180405(R) (2012).
[83] F. Du, K. Ohgushi, Y. Nambu, T. Kawakami, M. Avdeev, Y. Hirata, Y. Watanabe, T. J. Sato, and Y. Ueda, Stripelike magnetism in a mixed-valence insulating state of the Fe-based ladder compound $CsFe_2Se_3$, Phys. Rev. B **85**, 214436 (2012).
[84] J. M. Caron, J. R. Neilson, D. C. Miller, K. Arpino, A. Llobet, and T. M. McQueen, Orbital-selective magnetism in the spin-ladder iron selenides $Ba_{1-x}K_xFe_2Se_3$, Phys. Rev. B **85**, 180405(R) (2012).
[85] E. Dagotto, T. Hotta, and A. Moreo, Colossal magnetoresistant materials: The key role of phase separation, Phys. Rep. **344**, 1 (2021).
[86] J. Herbrych, N. Kaushal, A. Nocera, G. Alvarez, A. Moreo, and E. Dagotto, Spin dynamics of the block orbital-selective Mott phase, Nat. Commun. **9**, 3736 (2018).
[87] M. Daghofer, A. Nicholson, A. Moreo, and E. Dagotto, Three orbital model for the iron-based superconductors, Phys. Rev. B **81**, 014511 (2010).
[88] E. J. König, A. M. Tsvelik, and P. Coleman, Renormalization group analysis for the quasi-one-dimensional superconductor $BaFe_2S_3$, Phys. Rev. B **98**, 184517 (2018).
[89] R. M. Fernandes and A. V. Chubukov, Low-energy microscopic models for iron-based superconductors: A review, Rep. Prog. Phys. **80**, 014503 (2017).
[90] V. Cvetkovic and O. Vafek, Space group symmetry, spon-orbit coupling, and the low-energy effective Hamiltonian for iron-based superconductors, Phys. Rev. B **88**, 134510 (2013).
[91] V. Marino, A. Scazzola, F. Becca, M. Capone, and L. F. Tocchio, Intertwined superconductivity and orbital selectivity in a three-orbital Hubbard model for the iron pnictides, Phys. Rev. Lett. **134**, 196502 (2025).
[92] J. Rincón, A. Moreo, G. Alvarez, and E. Dagotto, Exotic magnetic order in the orbital-selective Mott regime of multiorbital systems, Phys. Rev. Lett. **112**, 106405 (2014).
[93] S. Li, N. Kaushal, Y. Wang, Y. Tang, G. Alvarez, A. Nocera, T. A. Maier, E. Dagotto, and S. Johnston, Nonlocal correlations in the orbital selective Mott phase of a one-dimensional multiorbital Hubbard model, Phys. Rev. B **81**, 014511 (2010).
[94] M. Uehara, T. Nagata, J. Akimitsu, H. Takahashi, N. Môri, and K. Kinoshita, Superconductivity in the ladder material $Sr_{0.4}Ca_{13.6}Cu_{24}O_{41.84}$, J. Phys. Soc. Jpn. **65**, 2764 (1996).
[95] T. Nagata, M. Uehara, J. Goto, J. Akimitsu, N. Motoyama, H. Eisaki, S. Uchida, H. Takahashi, T. Nakanishi, and N. Môri, Pressure-induced dimensional crossover and superconductivity in the hole-doped two-leg ladder compound $Sr_{14-x}Ca_xCu_{24}O_{41}$, Phys. Rev. Lett. **81**, 1090 (1998).
[96] L. F. Lin, N. Kaushal, C. Sen, A. D. Christianson, A. Moreo, and E. Dogotto, Oxygen magnetic polarization, nodes in spin density, and zigzag spin order in oxides, Phys. Rev. B **103**, 184414 (2021).
[97] S. Park, Y. J. Choi, C. L. Zhang, and S.-W. Cheong, Ferroelectricity in an $S = \frac{1}{2}$ chain cuprate, Phys. Rev. Lett. **98**, 057601 (2007).

[98] Y. Zhang, L.-F. Lin, A. Moreo, G. Alvarez, and E. Dagotto, Peierls transition, ferroelectricity, and spin-singlet formation in monolayer VOI_2, Phys. Rev. B **103**, L121114 (2021).
[99] J. Herbrych, G. Alvarez, A. Moreo, and E. Dagotto, Block orbital-selective Mott insulators: A spin excitation analysis, Phys. Rev. B **102**, 115134 (2020).
[100] J. Gooth, B. Bradlyn, S. Honnali, C. Schindler, N. Kumar, J. Noky, Y. Qi, C. Shekhar, Y. Sun, Z. Wang, B. A. Bernevig, and C. Felser, Axionic charge-density wave in the Weyl semimetal $(TaSe_4)_2I$, Nature (London) **575**, 315 (2019).
[101] Y. Zhang, L.-F. Lin, A. Moreo, and E. Dagotto, Orbital-selective Peierls phase in the metallic dimerized chain $MoOCl_2$, Phys. Rev. B **104**, L060102 (2021).
[102] http://energy.gov/downloads/doe-public-access-plan.
[103] 10.5281/zenodo.20360734.